Bayesian approach to image reconstruction in photoacoustic tomography

Jenni Tick[a], Aki Pulkkinen[a], and Tanja Tarvainen[a,b]

[a]Department of Applied Physics, University of Eastern Finland, P.O. Box 1627, 70211 Kuopio, Finland
[b]Department of Computer Science, University College London, Gower Street, London WC1E 6BT, United Kingdom

ABSTRACT

Photoacoustic tomography is a hybrid imaging method that has a variety of biomedical applications. In photoacoustic tomography, the image reconstruction problem (inverse problem) is to resolve the initial pressure distribution from detected ultrasound waves generated within an object due to an illumination of a short light pulse. In this work, this problem is approached in Bayesian framework. Image reconstruction is investigated with numerical simulations in different detector geometries, including limited view setup, and utilizing different prior information. Furthermore, assessing the reliability of the estimates is investigated. The simulations show that the Bayesian approach can produce accurate estimates of the initial pressure distribution and uncertainty information even in a limited view setup if proper prior information is utilized.

Keywords: photoacoustic tomography, inverse problems, Bayesian methods, uncertainty quantification

1. INTRODUCTION

Photoacoustic tomography (PAT),[1–4] also known as optoacoustic tomography, is a hybrid imaging modality that combines the advantages of pure optical and ultrasound imaging. In PAT, the region of tissue of interest is illuminated by a short pulse of visible or near-infrared light and the resulting ultrasound waves generated by the photoacoustic effect are collected by ultrasound detectors on the surface of the imaged target. From these time-varying ultrasound measurements, the initial pressure distribution is reconstructed utilizing an image reconstruction algorithm.

Several reconstruction algorithms have been utilized in photoacoustic image reconstruction.[5–15] Recently, utilizing a Bayesian approach in PAT was proposed.[16] Using the approach, estimates of the unknown parameters of interest (image reconstruction) can be provided together with information about the reliability of these estimates.

In this work, utilizing the Bayesian approach in PAT is investigated using numerical simulations. Utilizing different prior information is investigated. The approach is tested in different sensor geometries.

2. PHOTOACOUSTIC MODEL

When the optical energy of a short light pulse is absorbed by tissue, thermoacoustic effect leads to localized increase in acoustic pressure. This results in generation of a pressure wavefield which propagates through the medium to the surface of the object where it can be measured. This pressure propagation can be described by a linear, homogenous wave equation

$$\left(\frac{\partial^2}{\partial t^2} - c^2 \nabla^2 \right) p(r, t) = 0$$
$$p(r, t = 0) = p_0(r) \tag{1}$$
$$\frac{\partial}{\partial t} p(r, t = 0) = 0,$$

Further author information: (Send correspondence to J.T.)
J.T.: E-mail: jenni.tick@uef.fi, Telephone: +358 (0)50 564 3669

where p is the pressure, r is the spatial position, t is the time, c is the speed of sound and p_0 is the initial pressure distribution.[2–4] In practice, the measured pressure waves are polluted with noise, which is modeled as an additive noise in this work. The discrete observation model with an additive noise model for PAT is

$$p_t = Kp_0 + e, \tag{2}$$

where p_t is measured acoustic pressure waves, p_0 is the discrete initial pressure distribution, K is the discrete forward model which maps the initial pressure distribution to measurable data, and e denotes the noise. In this work, the matrix K is computed using the k-Wave toolbox[17] as described in Ref. 16.

3. BAYESIAN APPROACH

In the Bayesian approach,[18] all parameters are modeled as random variables. The solution of the inverse problem, the posterior density, is obtained based on the knowledge of the measurements, the model, and the prior information.

In the case of a linear observation model, an assumption that noise and initial pressure are mutually independent, and Gaussian distributed noise and prior, the posterior density is also a Gaussian distribution

$$p_0|p_t \sim \mathcal{N}(\eta_{p_0|p_t}, \Gamma_{p_0|p_t}) \tag{3}$$

where

$$\eta_{p_0|p_t} = (K^{\mathrm{T}}\Gamma_e^{-1}K + \Gamma_{p_0}^{-1})^{-1}(K^{\mathrm{T}}\Gamma_e^{-1}(p_t - \eta_e) + \Gamma_{p_0}^{-1}\eta_{p_0}) \tag{4}$$

$$\Gamma_{p_0|p_t} = (K^{\mathrm{T}}\Gamma_e^{-1}K + \Gamma_{p_0}^{-1})^{-1} \tag{5}$$

are the mean and covariance, respectively, where η_e and Γ_e are the mean and covariance matrix characterizing the noise, and η_{p_0} and Γ_{p_0} are the mean and covariance matrix of the prior information.

A reconstructed image of an initial pressure distribution is obtained by calculating point estimates of the posterior density such as *maximum a posteri* (MAP) estimate. In a purely Gaussian case, the MAP estimate is the (conditional) mean of the posterior distribution $p_{0,\mathrm{MAP}} = \eta_{p_0|p_t}$. Standard deviations σ for the estimates can be computed by taking the square root of the diagonal elements of the posterior covariance matrix $\Gamma_{p_0|p_t}$.

3.1 Prior Information

Prior expresses what is known about the unknown parameter of interest before any experiments are carried out. In this work, three different Gaussian priors and their impact on the solution are investigated. The priors utilized are the white noise prior, Ornstein-Uhlenbeck process and squared exponential prior.[19]

The white noise prior assumes that the estimated parameters are independent of each other or have no spatial correlation. It is well suited for the estimation of parameters which have a non-smooth spatial distribution. In the white noise prior, the covariance matrix is a diagonal matrix with the values of variance $\sigma_{p_0}^2$ on the diagonal

$$\Gamma_{p_0} = \sigma_{p_0}^2 I. \tag{6}$$

Contrary to the white noise prior, the squared exponential is an appropriate prior for spatially smooth (strongly correlated) parameters. In the squared exponential prior, the covariance matrix is of form

$$\Gamma_{p_0,ij} = \sigma_{p_0}^2 \exp\left(-\frac{\|r_i - r_j\|^2}{2l^2}\right) \tag{7}$$

where i and j are the pixel indices, r_i and r_j are the corresponding pixel positions, $\sigma_{p_0}^2$ is the variance and l is the characteristic length scale which controls the spatial range of correlation.

The Ornstein-Uhlenbeck prior can be seen as a compromise between the white noise and squared exponential priors. It is not as smooth as the squared exponential prior but it still supports correlation between the pixels.

Therefore, the Ornstein-Uhlenbeck prior promotes distributions that can be locally close to homogeneous with sharp changes between different areas. The covariance matrix of the Ornstein-Uhlenbeck prior is defined as

$$\Gamma_{p_0,ij} = \sigma_{p_0}^2 \exp\left(-\frac{\|r_i - r_j\|}{l} \right),\tag{8}$$

where $\sigma_{p_0}^2$ is the variance and l is the characteristic length scale as in the case of the squared exponential prior. The Ornstein-Uhlenbeck process is a special case of Matérn covariance functions obtained by setting the smoothness parameter to 0.5.

4. NUMERICAL SIMULATIONS

The Bayesian approach was investigated with numerical simulations. The simulated domain was a circle of 4 mm diameter. Medium was assumed to be non-attenuating with a constant speed of sound $c = 1500$ m/s.

Two different kind of initial pressure distributions were examined. In the first problem, the true simulated initial pressure distribution contained five disks of 0.43 mm radius on a homogenous background. Initial pressure on the disks was 10 and the background was set to zero. In the second problem, the disks were Gaussian distributions with a peak value of 4, and a full-width half-maximum of 0.4 mm.

Two sets of sensor geometries were considered. In the first setup, the acoustical sensors were evenly distributed on a circle of 4.5 mm diameter and the number of sensors was 180, 60, 30 and 15. In the second setup, the acoustical sensors spanned an angular interval of 360, 180, 60 and 32 degrees on a circle of 4.5 mm diameter and the number of sensors was 180, 90, 30 and 16.

The data was simulated using the k-space time domain method implemented with the k-Wave MATLAB toolbox.[17] The pressure signals were recorded for 7 μs at 100 MHz (701 temporal samples). The simulated pressure signals were corrupted by uncorrelated Gaussian distributed noise with zero mean and a standard deviation proportional to 1% of the peak amplitude of the simulated pressure signal. In discretization, a pixel width $\Delta h = 14.29\,\mu$m was used.

In the inverse problem, the target domain has different discretization ($\Delta h = 25\,\mu$m) to avoid an inverse crime. The matrix K was formed utilizing k-Wave toolbox as in Ref. 16. As prior information, the white noise, Ornstein-Uhlenbeck and squared exponential priors were used. The means of the priors were set to the value of the background and the standard deviations were set to 3.5. For the Ornstein-Uhlenbeck and squared exponential priors, the characteristic length scale $l = 0.125$ mm was used. The measurement noise was considered to be uncorrelated Gaussian distributed noise with zero mean and the standard deviation set to 1% of the peak positive amplitude of the noisy simulated data.

The MAP estimates of the initial pressure distribution $p_{0,\text{MAP}}$ were computed using Eq. (4). Standard deviations were determined as described in Sec. 3 using Eq. (5).

4.1 Results

The true initial pressure distribution, the MAP estimates and their standard deviations in the case of the uniform disks are shown in Fig. 1 for the different full view sensor geometries and in Fig. 2 for the different limited view sensor geometries. As it can be seen, the estimates match the true initial pressure distribution, when the sensors are densely around the object. In this case, the standard deviations are small meaning that the uncertainty of the estimates is small. When the number of the sensors is decreased, the quality of the estimates is reduced. Decreasing the number of sensors also increases the standard deviations, which indicates that uncertainty of the estimates increases. If sensor geometry turns more limited view, the quality of the estimates severely reduces, especially in the areas which are not enclosed by sensors. In those areas, artefacts and distortions can be seen. Also the standard deviations increase in the limited view setups. The increase of the standard deviation is more significant in the areas outside the region enclosed by the sensors. Comparing the estimates obtained using different priors, it can be seen that the MAP estimates obtained using the Ornstein-Uhlenbeck and squared exponential priors are very similar in quality and they look better than the estimates obtained using the white noise prior. This is especially evident in the visibility of the lower inclusions in Fig. 2. This difference is more
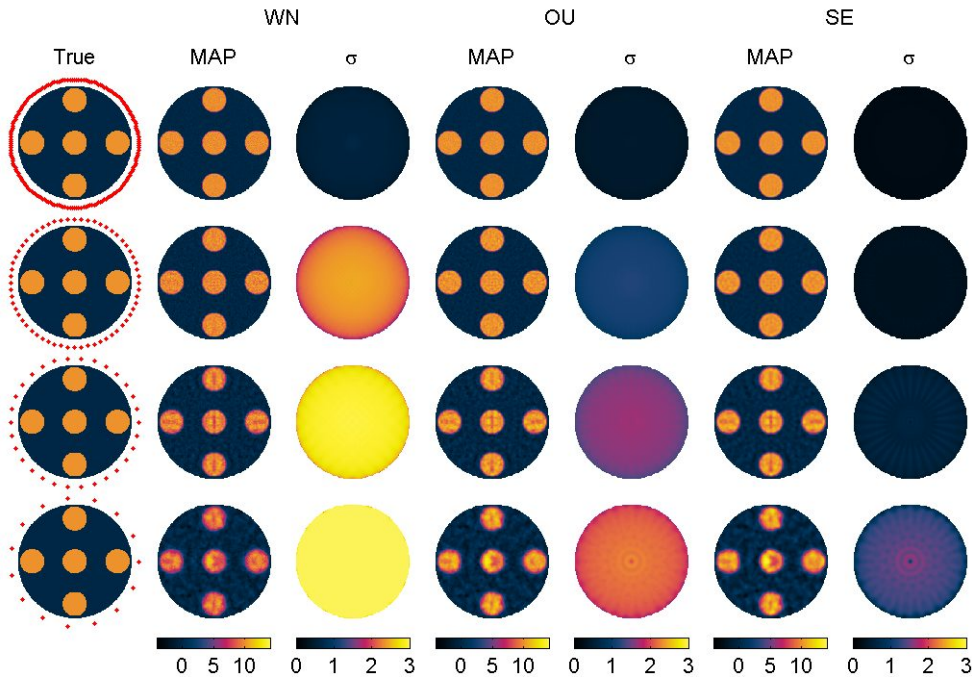
Figure 1. The true initial pressure distribution, the MAP estimates and their standard deviations σ obtained using the white noise prior (WN), Ornstein-Uhlenbeck prior (OU) and squared exponential prior (SE) in different full view sensor geometries in the case of the uniform disks. The dots indicate the locations of the sensors.
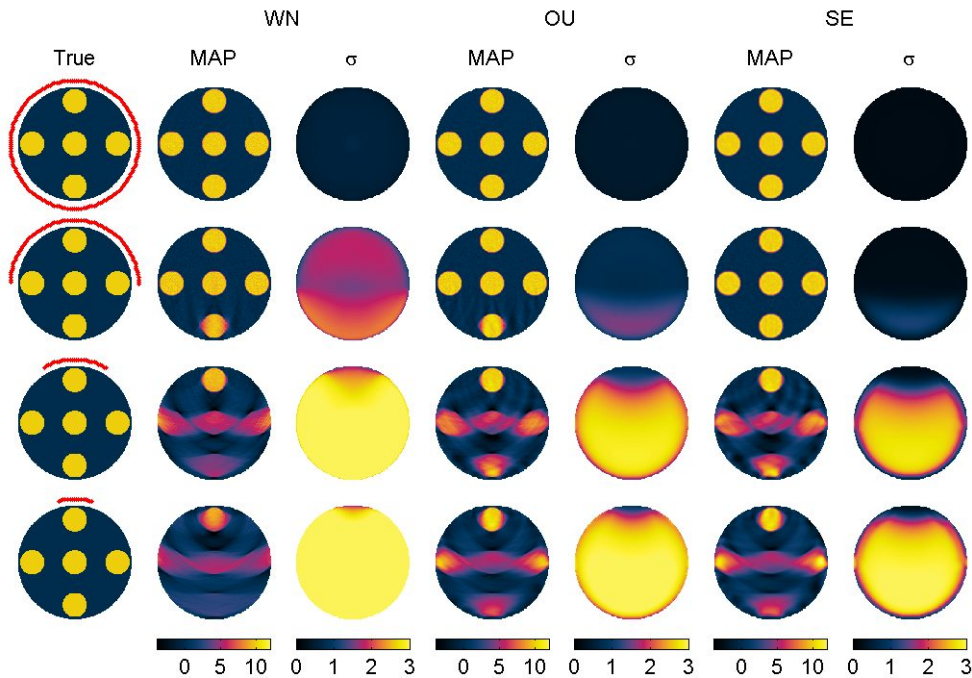

Figure 2. The true initial pressure distribution, the MAP estimates and their standard deviations σ obtained using the white noise prior (WN), Ornstein-Uhlenbeck prior (OU) and squared exponential prior (SE) in different limited view sensor geometries in the case of the uniform disks. The dots indicate the locations of the sensors.
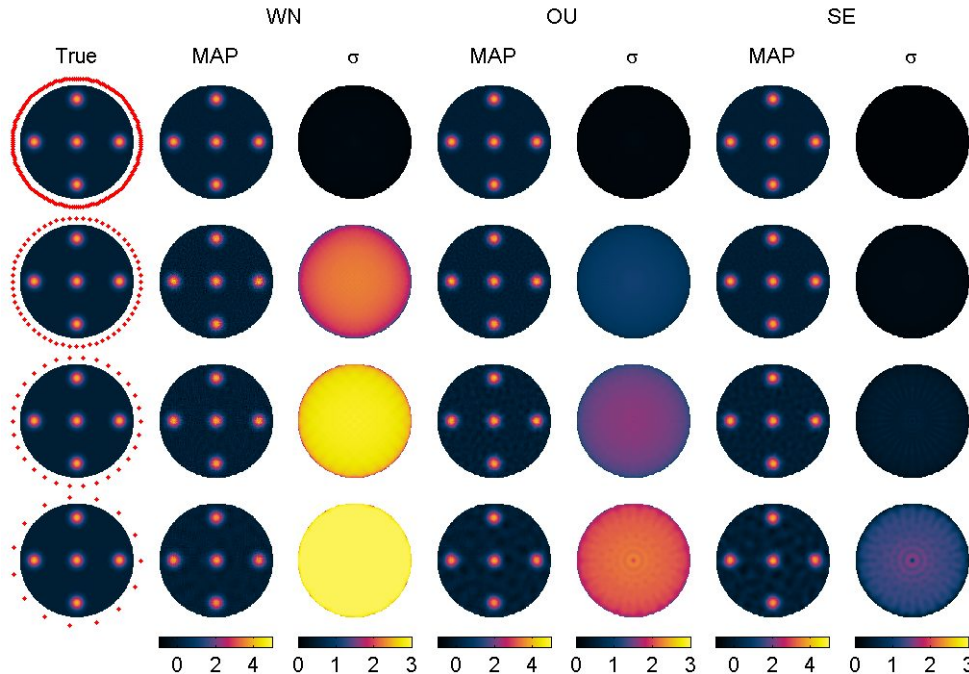
Figure 3. The true initial pressure distribution, the MAP estimates and their standard deviations σ obtained using the white noise prior (WN), Ornstein-Uhlenbeck prior (OU) and squared exponential prior (SE) in different full view sensor geometries in the case of the Gaussian disks. The dots indicate the locations of the sensors.

apparent in the limited view reconstructions. Also the standard deviations obtained using different priors are different.

The true initial pressure distribution, the MAP estimates and their standard deviations in the case of the Gaussian disks are shown in Fig. 3 for the different full view sensor geometries and in Fig. 4 for the different limited view sensor geometries. As it can be seen, the results obtained using the Gaussian disks are very similar to the results obtained using the uniform disks. The best quality estimates and the smallest standard deviations are obtained when sensors are located densely around the object. Similarly as in the case of the uniform disks, the quality of the estimates reduces and the standard deviations increase if the number of the sensors is decreased. Differences between the estimates obtained using the different priors are almost indistinguishable in the full view sensor geometries. In the limited view setups, the estimates obtained using the Ornstein-Uhlenbeck and squared exponential priors are better than estimates obtained using the white noise prior. The largest standard deviations are obtained using the white noise prior and the smallest standard deviations are obtained using the squared exponential prior.

5. CONCLUSIONS

The Bayesian approach to photoacoustic tomography image reconstruction with uncertainty quantification was investigated in the presence of different prior information. MAP estimates and standard deviations were computed from simulated data in various sensor geometries. The results showed that the sensor geometry affected both the estimates and the reliability of the estimates. In the full view setups, the visual appearance of estimates stayed approximately same, but uncertainties increased when the number of the sensors was reduced. In the limited view setups, the quality of the estimates reduced and the uncertainty increased, especially in the areas outside the region enclosed by the sensors. It could be seen that accurate prior information is needed for proper estimates and reliable uncertainty quantification, especially in a limited view case. However, more research is required for interpretation of when uncertainty estimates can be regarded safe, see e.g. Ref. 20
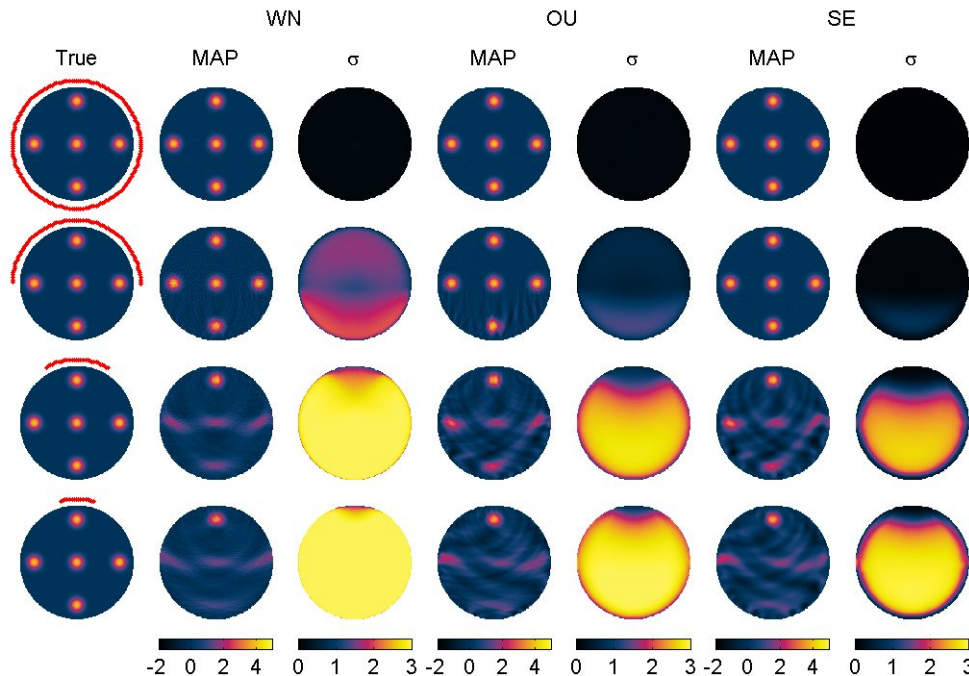
Figure 4. The true initial pressure distribution, the MAP estimates and their standard deviations σ obtained using the white noise prior (WN), Ornstein-Uhlenbeck prior (OU) and squared exponential prior (SE) in different limited view sensor geometries in the case of the Gaussian disks. The dots indicate the locations of the sensors.

REFERENCES

[1] Beard, P., "Biomedical photoacoustic imaging," *Interface Focus* **1**(4), 602–631 (2011).

[2] Li, C. and Wang, L. V., "Photoacoustic tomography and sensing in biomedicine," *Physics in Medicine and Biology* **54**(19), R59–R97 (2009).

[3] Lutzweiler, C. and Razansky, D., "Optoacoustic imaging and tomography: Reconstruction approaches and outstanding challenges in image performance and quantification," *Sensors (Switzerland)* **13**(6), 7345–7384 (2013).

[4] Xu, M. and Wang, L. V., "Photoacoustic imaging in biomedicine," *Review of Scientific Instruments* **77**(4), 041101 (2006).

[5] Agranovsky, M. and Kuchment, P., "Uniqueness of reconstruction and an inversion procedure for thermoacoustic and photoacoustic tomography with variable sound speed," *Inverse Problems* **23**(5), 2089–2102 (2007).

[6] Kunyansky, L. A., "A series solution and a fast algorithm for the inversion of the spherical mean Radon transform," *Inverse Problems* **23**(6), S11–S20 (2007).

[7] Xu, M. and Wang, L. V., "Universal back-projection algorithm for photoacoustic computed tomography," *Physical Review E - Statistical, Nonlinear, and Soft Matter Physics* **71**(1), 016706 (2005).

[8] Finch, D., Patch, S. K., and Rakesh, "Determining a function from its mean values over a family of spheres," *SIAM Journal on Mathematical Analysis* **35**(5), 1213–1240 (2004).

[9] Burgholzer, P., Matt, G. J., Haltmeier, M., and Paltauf, G., "Exact and approximative imaging methods for photoacoustic tomography using an arbitrary detection surface," *Physical Review E - Statistical, Nonlinear, and Soft Matter Physics* **75**(4), 046706 (2007).

[10] Hristova, Y., Kuchment, P., and Nguyen, L., "Reconstruction and time reversal in thermoacoustic tomography in acoustically homogeneous and inhomogeneous media," *Inverse Problems* **24**(5), 055006 (2008).

[11] Deán-Ben, X. L., Buehler, A., Ntziachristos, V., and Razansky, D., "Accurate model-based reconstruction algorithm for three-dimensional optoacoustic tomography," *IEEE Transactions on Medical Imaging* **31**(10), 1922–1928 (2012).

[12] Rosenthal, A., Razansky, D., and Ntziachristos, V., "Fast semi-analytical model-based acoustic inversion for quantitative optoacoustic tomography," *IEEE Transactions on Medical Imaging* **29**(6), 1275–1285 (2010).

[13] Zhang, J., Anastasio, M. A., Rivire, P. J. L., and Wang, L. V., "Effects of different imaging models on least-squares image reconstruction accuracy in photoacoustic tomography," *IEEE Transactions on Medical Imaging* **28**(11), 1781–1790 (2009).

[14] Paltauf, G., Viator, J. A., Prahl, S. A., and Jacques, S. L., "Iterative reconstruction algorithm for optoacoustic imaging," *Journal of the Acoustical Society of America* **112**(4), 1536–1544 (2002).

[15] Wang, K., Su, R., Oraevsky, A. A., and Anastasio, M. A., "Investigation of iterative image reconstruction in three-dimensional optoacoustic tomography," *Physics in Medicine and Biology* **57**(17), 5399–5423 (2012).

[16] Tick, J., Pulkkinen, A., and Tarvainen, T., "Image reconstruction with uncertainty quantification in photoacoustic tomography," *The Journal of the Acoustical Society of America* **139**(4), 1951–1961 (2016).

[17] Treeby, B. E. and Cox, B. T., "k-wave: Matlab toolbox for the simulation and reconstruction of photoacoustic wave fields," *Journal of Biomedical Optics* **15**(2), 021314 (2010).

[18] Kaipio, J. and Somersalo, E., [*Statistical and Computational Inverse Problems*], Springer Science & Business Media (2006).

[19] Rasmussen, C. E. and Williams, C. K. I., [*Gaussian Processes for Machine Learning*], MIT Press (2006).

[20] Pulkkinen, A., Cox, B. T., Arridge, S. R., Goh, H., Kaipio, J. P., and Tarvainen, T., "Direct estimation of optical parameters from photoacoustic time series in quantitative photoacoustic tomography.," *IEEE transactions on medical imaging* **35**(11), 2497 (2016).